THz Thermal Radiation Enhancement Using an Electromagnetic Crystal

Hao Xin, *Senior Member, IEEE*, Ziran Wu, Abram Young, and Richard Ziolkowski, *Fellow, IEEE*

***Abstract*—Thermal radiation in the terahertz (THz) range only occupies a tiny portion of the whole blackbody power spectrum at room temperature. We demonstrate that a thermal radiator, which is constructed from an electromagnetic (EM) crystal, can be designed so that its photon density of states (DOS) is enhanced in the THz frequency range. We also demonstrate, as a consequence, that this source may lead to large enhancements of the radiated power over the values associated with normal blackbody radiation at those frequencies. The THz thermal radiation enhancement effects of various EM crystals, including both silicon and tungsten woodpile structures and a cubic photonic cavity (CPC) array, are explored. The DOS of the woodpile structures and the CPC array are calculated, and their thermal radiation intensities are predicted numerically. These simulations show that the radiated power can be enhanced by a factor of 11.8 around 364 GHz and 2.6 around 406 GHz, respectively, for the silicon and tungsten woodpile structures in comparison to the normal blackbody radiation values at those frequencies. It is also shown that an enhancement factor of more than 100 may be obtained by using the CPC array. A silicon woodpile EM crystal with a band gap around 200 GHz was designed and fabricated. The transmission property of this woodpile structure was verified using the THz time-domain spectroscopy (TDS). Thermal emissions from the fabricated silicon woodpile and a control blackbody sample were measured. Enhancements of the woodpile source radiation over the blackbody were observed at several frequencies which are consistent with the theoretical predictions.**

***Index Terms*—Blackbody radiation, density of states (DOS), electromagnetic (EM) crystal, terahertz.**

I. Introduction

THE terahertz (THz) portion of the frequency spectrum, 3×10^{11}–3×10^{12} Hz, is currently underutilized and may be very important for many applications in the near future, including remote sensing, imaging, and communications [1]. These frequencies combine some of the advantages of both the microwave and infrared (IR) spectra, i.e., they provide coverage in IR-blind conditions while offering more bandwidth and resolution than is available with microwave frequencies. As a result, THz technology has experienced a renaissance over the past few years. While continuing to make major strides in sub-millimeter wave astronomy and remote sensing, THz technology is blooming with potential applications in contraband detection, tumor recognition, DNA sequencing, tissue imaging, radar and communications [1]–[7]. However, the availability of THz sources remains one of the major bottlenecks in the realization of the promises of THz technology for many of these exciting applications. Conventional tube sources are cumbersome, require high-voltage power supplies, necessitate high internal electric and magnetic field intensities, and have reliability and life time issues [8]. Conventional IR pumped laser sources are also bulky, have a limited tuning range, and are expensive [9]. Traditional electronic solid-state sources suffer from reactive parasitics, and the transit time of the carriers causes high frequency roll-offs [1]. Moreover, optical type sources, such as solid-state lasers, are not suitable for THz frequencies due to the comparable photon and lattice phonon energies [1]. One of the most popular methods currently used for generating THz power is frequency conversion: either up-conversion from millimeter wavelengths by frequency multipliers made of nonlinear capacitors such as heterostructure barrier varactor (HBV) diodes and planar Schottky diodes [10]–[12], or down-conversion from optical or IR frequencies through laser heterodyning or photomixing [13]. Both of these frequency conversion approaches have been proven to be inefficient. In this paper, we introduce a potential THz source that is based on the thermal radiation enhancement enabled by electromagnetic or photonic crystals. The term "photonic crystal" is more strictly associated with infrared and optical frequencies, while the terms electromagnetic (EM) crystal and electromagnetic band gap (EBG) structure are more general and cover all frequencies, including the THz range. They refer to the same behavior since there is a physical equivalence between electromagnetic waves and photon modes. We will use both of the more general terms, EM crystal and EBG structure, in our discussion below. Preliminary theoretical and experimental results are reported and give promising indications that a new type of thermal THz source may be realized using carefully designed EM crystal thermal radiators.

The inspiration for this THz source concept comes from a well known idea that a three-dimensional EM crystal can drastically modify the spontaneous emission spectra from an atomic or a semiconductor material via the redistribution of the photon density of states (DOS) in different frequency ranges. Within the

Manuscript received March 17, 2008; revised May 24, 2008. Published September 4, 2008 (projected). This work was supported in part by NSF Award 0823864. The work of H. Xin was supported in part by the ARO under Contract W911NF0610087 and the work of R. Ziolkowski was supported in part by DARPA under Contract HR0011-05-C-0068.

H. Xin is with the Electrical and Computer Engineering Department and the Physics Department, University of Arizona, Tucson, AZ 85721-0104 USA (e-mail: hxin@ece.arizona.edu).

Z. Wu is with the Department of Physics, University of Arizona, Tucson, AZ 85721-0104 USA.

A. Young is with the Department of Physics, University of Arizona, Tucson, AZ 85721-0104 USA and also with TeraVision, Inc., Tucson, AZ 85705-2203 USA.

R. Ziolkowski is with the Department of Electrical and Computer Engineering and the College of Optical Sciences, University of Arizona, Tucson, AZ 85721-0104 USA (e-mail: ziolkowski@ece.arizona.edu).

Color versions of one or more of the figures in this paper are available online at http://ieeexplore.ieee.org.

Digital Object Identifier 10.1109/TAP.2008.928806

EBG of an EM crystal, spontaneous emission is completely forbidden because there is no photon state in that frequency range which can couple with an atomic transition, yielding a photon DOS that is zero. Outside the EBG, the emission rate is directly correlated with the photon DOS [14]. The existence of an EBG will result in a shift of the emission energy from the forbidden frequency range to another adjacent EM band-pass frequency range. This in turn causes an enhanced DOS to emerge and, hence, an enhanced emission rate there. This phenomenon is often known as the "anti-crossing" effect. To the first order (assuming ideal coupling to the external environment), thermal radiation emitted by an object has a linear relationship with its photon DOS. Consequently, a thermal radiation enhancement can be expected in a frequency range for which the photon DOS is much higher than that of a normal black body. This phenomenon has been explored both theoretically and experimentally [14]–[17]. For example, both passive experiments using one-dimensional or three-dimensional EM crystals as filters [18], [19], and active experiments using EM crystals directly as a radiation source [17], [20], have been reported. Possible interpretations of the underlying physics of the thermal radiation enhancement, and direct calculations based on these interpretations [16], [17], [21]–[23] have been reported. Some controversy still remains with these results [24]. However, while previous work focused mainly on IR and optical wavelengths, the goal here is to explore this phenomenon in the THz frequency range.

In this paper, we explain the principles of thermal radiation enhancement enabled by EBG structures. A brief overview of current research on thermal radiation from EBG materials is given. We then present theoretical calculations of the thermal radiation spectra of several EBG structures used as active sources. The numerically predicted DOS of these structures and the associated enhancements of the radiated thermal power over the normal blackbody radiation values in certain frequency regimes are given. The fabrication and testing results, including direct active emission measurements of a silicon woodpile structure, are then presented. Finally, possible future work, including multiband EBG structures for greater enhancements and tunable EBG structures, is proposed.

II. Theoretical Principles

Artificially engineered EM crystals consist of periodic dielectric and/or metallic structures. Because of their periodicity, these structures have unique electromagnetic properties, such as the existence of band gaps and a photon density-of-states (DOS), which are analogous to semiconductor energy band gaps and the electron DOS. Since the physics of an EM crystal is highly scalable in frequency, EBG-based devices have already shown promise as effective methods for controlling and manipulating wave-propagation for both microwave and optical frequencies [25]. Lately more attention has been devoted to EBG-based devices in the THz regime [26] due to increased scientific and engineering interests [27] in THz sensing, imaging, and communication areas. Besides controlling and manipulating the propagation of EM waves through wave-EM crystal interactions, EBG structures can also be used to alter and tailor EM processes such as the emission and detection of EM radiation. For example, spontaneous emission may be inhibited [28] or enhanced. The possibility of designing EBG structures to manipulate the final states of electromagnetic processes may have significant implications in many physical, chemical, and biological processes in nature.

Blackbody radiation has been a subject of interest since the beginning of the past century due to Planck [29]. The thermal power radiated by a normal blackbody at temperature T (degrees Kelvin) within the frequency range f to $(f+df)$ (Hz) per unit volume is well defined by the free space Planck's equation

$$u(f)df = \rho(f)\cdot\frac{hf}{e^{hf/kT}-1}\cdot df = \frac{8\pi f^2}{c^3}\cdot\frac{hf}{e^{hf/kT}-1}\cdot df \quad (1)$$

where $\rho(f)$ is the photon density of states, $h = 6.626e-34$ m^2kg/s is the Planck constant, hf is the individual photon energy, $k = 1.381e-23\ J/K$ is the Boltzmann constant, and the term $1/[exp(hf/kT)-1]$ is the Bose-Einstein distribution representing the photon statistics. At room temperature, (1) predicts that the blackbody radiation peak will occur at IR frequencies, while the radiated power in the THz range will occupy only a tiny portion of the entire blackbody power spectrum. However, it is conceivable that the Planck distribution could be modified if the emitting object is an EM crystal and its photon DOS is different than the one typically associated with a normal blackbody object. In (1), all quantities are fixed except the overall photon DOS $\rho(f)$. To modify the thermal radiation of an object, a nontrivial redistribution of the DOS is required. Thus, the idea of modifying the normal blackbody DOS with a three-dimensional (3D) EM crystal arises naturally, following the general rule of thumb that the presence of a complete EBG usually means a drastic redistribution of the photon DOS into different frequency regions [14].

A passive approach to modify spontaneous emission is to use the EM crystal as a filter, i.e., the source emission spectrum is reshaped corresponding to the passband/stopband characteristics of the EM crystal [19]. On the other hand, spontaneous emission directly from atoms in the EM crystal itself, i.e., the EM crystal is the active emission source, is yet another approach. Previous theoretical [14] and experimental [30] work have indicated that the thermal emission from an EBG structure could indeed be different than the Planck distribution and, in certain frequency bands, the output intensity could be higher than that emitted by a normal blackbody. In some experiments [24], [30], a controversial effect that seemingly violates the second law of thermodynamics was reported. For example, the levels of thermal emission from a tungsten woodpile structure (WPS) were shown to exceed its absorption dramatically. This behavior contradicts the Kirchoff's Law, i.e., for an object in thermal equilibrium, its thermal emission at any frequency should not exceed the value defined by the Planck curve [22]–[24]. The explanation for this contradiction was that the WPS may not be in thermal equilibrium [31]. Several other theoretical works have confirmed that enhanced thermal emission would occur when the EM crystal is not in thermal equilibrium [16], [17]. In summary, there have been a series of experimental studies on thermal emission from metallic WPSs; and their results are not all consistent [17], [30], [32]–[35]. The key controversy is whether the metallic WPS emission enhancement over the blackbody values has actually

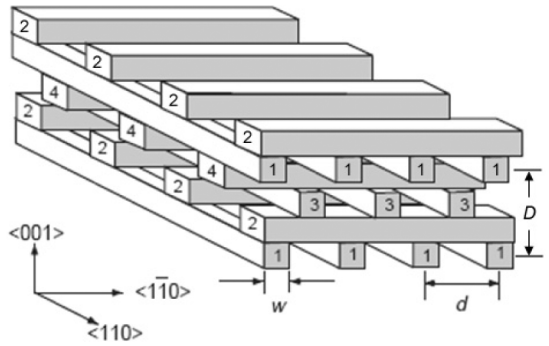

Fig. 1. Schematic drawing of a woodpile EM crystal.

been observed experimentally [17], [30], [32] or not [33]–[35]. Nonetheless, the focus of all previous work has been in the near-IR regime and has targeted light source applications. This investigation of thermal emission from an EBG structure in the THz regime contributes to the understanding of the fundamental properties of EM crystals and may lead to useful THz applications.

III. Design and Calculation of Several EBG Structures

Three structures are commonly known to have complete 3-D EBGs: inverse-opal, diamond, and woodpile structures. The WPS (also named the Lincoln-Log structure [17] because its relatively simple geometry is related to structures attainable with Lincoln-Log building toy sets) is selected for our study here. A drawing of a WPS is shown in Fig. 1, [36]; it consists of a unit cell containing 4 layers of infinitely long silicon square rods stacked with a periodicity D. Within the unit cell, the rods in each layer are distributed with the same periodicity d; and the adjacent layers that have the same rod orientation are shifted with respect to each other by $d/2$. Each rod has a height $h = D/4$ and a width $w = h$. Thus, the filling ratio of the rods with respect to the whole structure is equal to w/d. This EM crystal can be treated as a face-centered-tetragonal (fct) or a simple tetragonal (st) lattice. In this case, the simple tetragonal lattice whose unit cell contains four attached rods with periodicity d in the $\langle 110\rangle$ and $\langle 1\bar{1}0\rangle$ lattice directions and periodicity D in the $\langle 001\rangle$ stacking direction (see Fig. 1) is considered. The center frequency of the WPS band gap is scalable by its lattice parameters. By varying the WPS filling ratio, its band gap width can also be adjusted.

A. Silicon Woodpile Structure

The photon DOS of a silicon (with a refractive index 3.40) WPS designed with $w/d = 0.272$ and $D/d = 1.089$, is plotted in Fig. 2(a). The DOS is obtained by determining the eigenmodes of the WPS within the irreducible Brillouin zone of the lattice. The computation code MIT MPB [37] was used for the calculation of the eigenmodes. The DOS was then generated with a numerical interpolation method [38], [39], which is based on all of the eigenmode frequencies obtained as the k-points sweep the irreducible Brillouin zone. Notice that the abscissa of Fig. 2(a) is the normalized frequency x, which is related to the absolute frequency as $x = (a/c)f = d \cdot f/c$, where c is the speed of light in vacuum, and $a = d$ is the st-lattice constant. Therefore, a simple scaling of d can fit the response of the whole structure into any frequency band of practical interest. The ordinate is the photon DOS $\rho(x)$ at the normalized frequency x. The transformation from the DOS at the normalized frequency, $\rho(x)$, to the DOS at the real frequency, $\rho(f)$, is given by the relation: $\rho(f) = \rho(x)(1/ca^2)$. The thermal radiation power per unit surface area per unit frequency $j(f)$ is

$$j(f) = \int_0^{2\pi} d\varphi \int_0^{\pi/2} d\theta \cdot \frac{c}{4\pi} u(f) \cos\theta \sin\theta = u(f) \cdot c/4. \tag{2}$$

Using the expression of $u(f)$ in (1) and the relation between $\rho(f)$ and $\rho(x)$, $j(f)$ is explicitly given by the expression

$$j(f) = \frac{hcf\rho(f)}{4(e^{hf/kT} - 1)} = \frac{hcx\rho(x)}{4a^3(e^{hcx/akT} - 1)}. \tag{3}$$

The corresponding formula that is used to calculate the radiation power density of a normal blackbody is

$$j_0(f) = \frac{2\pi hf^3}{c^2(e^{hf/kT} - 1)} = \frac{2\pi hcx^3}{a^3(e^{hcx/akT} - 1)}. \tag{4}$$

The computed j for the silicon WPS having the rod periodicity $d = 646$ μm and the computed j_0 for room temperature are plotted in Fig. 2(b) versus the real frequency. The center of the band gap is determined to be 195 GHz. With these calculations, an enhancement factor of j/j_0 can be defined. This thermal emission power enhancement factor for the silicon WPS is plotted in Fig. 2(c). Those results illustrate how the silicon woodpile EM crystal may greatly modify the thermal power emitted within a specific portion of the THz frequency range.

The plots in Fig. 2 explicitly show a complete band gap from around 175 to 216 GHz, i.e., there is no thermal energy radiated in that frequency band. The photon DOS gaps, peaks, and consequently the modified thermal radiation power at these frequencies originate from Bragg diffractions in between the EM crystal lattice layers. For example, the DOS peaks can be regarded as the Bragg diffraction resonances. In particular, there are several thermal radiation power enhancement peaks observed, for example, around 148, 163, 254, 283, 364, 393, 415 and 448 GHz. The power enhancement factor is as high as 11.8 at the 364 GHz peak, which means there is more than 1080% power output increase at 364 GHz over the normal blackbody value.

To verify the accuracy of these numerical results, an alternative method was developed to calculate the WPS eigenmodes. In particular, we used the commercial 3-D finite-element electromagnetics solver from ANSOFT, the High Frequency Structure Simulator (HFSS), to calculate the eigenmodes of the same silicon WPS [40]. Although much more computationally intensive, one valuable benefit of using the HFSS Eigen-solver, in contrast to the MPB code, is that it can handle lossy structures, for example, a lossy dielectric or a metallic EM crystal. The same silicon lossless WPS structure that was modeled with the

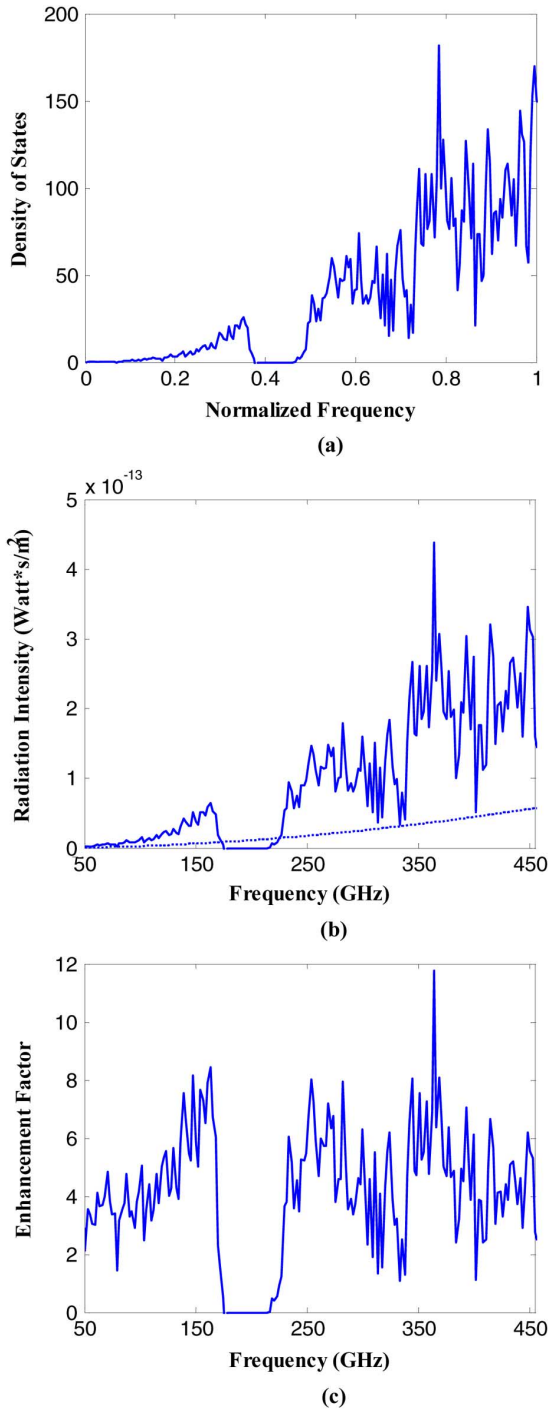

Fig. 2. (a) Calculated photon density of states of the silicon woodpile structure, which has the filling ratio $w/d = 0.272$, and $D/d = 1.089$. The refractive index of the rods is $n = 3.40$ (silicon). The normalized frequency is given by $x = (a/c) = d \cdot f/c$. (b) Predicted radiation power intensities of the woodpile (solid) and the normal blackbody (dotted) at room temperature. (c) Thermal radiation power enhancement factor.

MPB code, was modeled again with the HFSS Eigen-solver. The HFSS Master/Slave boundary conditions are applied on the tetragonal unit cell surfaces to sweep the corresponding k-space in the irreducible Brillouin zone, with the same sweeping density as the MPB simulation. After the completion of the HFSS simulation, the eigenmode data is collected and the same interpolation method mentioned previously is used to compute the

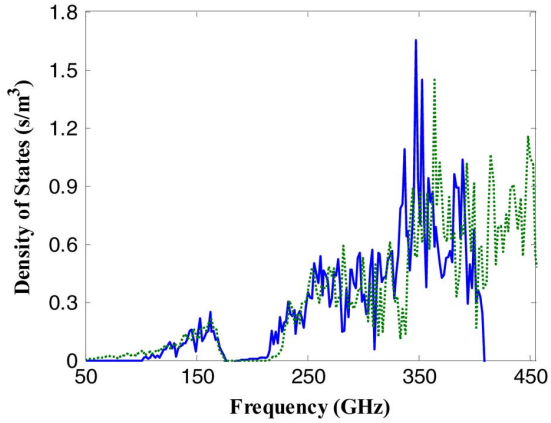

Fig. 3. The real frequency DOS obtained using the HFSS Eigen-solver (solid line) and the MPB (dashed line) for the silicon woodpile structure with the filling ratio $w/d = 0.272$, $D/d = 1.089$, and the rod periodicity $d = 646\ \mu$m.

photon DOS. The resulting DOS is plotted in Fig. 3. The MPB results shown in Fig. 2(a) (converted to the real frequency DOS $\rho(f)$ by using the formulas presented above, with the lattice constant $a = 646\ \mu$m) are also plotted in Fig. 3 for comparison purpose. In general, they match well with the HFSS-simulated DOS especially that most of the DOS peaks line up between the two methods. It can also be seen that there is some difference between the HFSS and the MPB results, for example, the slight shift of the main enhancement peak position and the small band gap width difference in Fig. 3. The discrepancies are probably due to the following reasons. First, only 52 bands are included in the HFSS simulation approach (notice that the HFSS simulations were stopped around 400 GHz) because of limited computing resources. In contrast, the MPB simulation method includes 90 bands. Second, the strong Bragg resonances that result in the band gap may degrade the HFSS Eigen-solver calculation accuracy. Nevertheless, the agreement between the MPB and HFSS results shown in Fig. 3 is still quite reasonable in terms of both the band gap position and the relative values of the DOS peaks. In the cases of the tungsten WPS and the photonic cavity discussed in later sections, HFSS is the only software available to us that can deal with metallic and lossy dielectric structures. The fact that the HFSS and MPB computed DOS for the silicon WPS agreed reasonably well serves as a validation of using HFSS to compute the DOS of the tungsten WPS and the Q factor of the photonic cavity.

B. Tungsten Woodpile Structure

One significant advantage of building a WPS with metal is that the structure can be easily heated by applying an electrical current to it. This would also lead to thermal emission power at much higher levels than at the room temperature. Moreover, because silicon oxidizes when its temperature reaches 800°–1200°C in an atmosphere that contains oxygen or water vapor [41], its oxidation prevents it from being heated to higher temperatures, as would be desirable for a potential thermal source.

The DOS of a tungsten WPS was calculated using the HFSS Eigen-solver approach. Tungsten has a bulk conductivity $\sigma = 1.82e7$ Siemens/m. The designed tungsten WPS has a filling

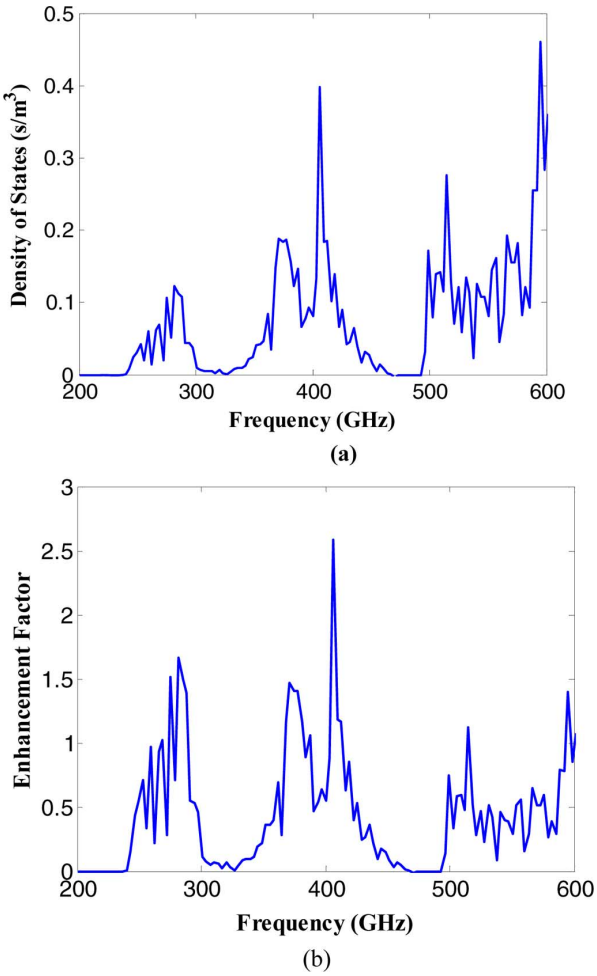

Fig. 4. (a) Calculated photon DOS for the tungsten woodpile structure with the filling ratio $w/d = 0.272$, $D/d = 1.089$, and the periodicity $d = 646$ μm. (b) Thermal radiation power enhancement factor for this tungsten WPS.

ratio $w/d = 0.272, D/d = 1.089$, and a lattice constant $d = 646$ μm, which are the same as the silicon WPS discussed in Section A. The simulation results for the tungsten WPS DOS and the thermal radiation power enhancement factor are plotted in Fig. 4(a) and (b), respectively. A complete band gap can be seen between 470 and 493 GHz. In comparison to the silicon WPS with exactly the same geometry, the gap center frequency is blue shifted and the overall gap is narrower. From Fig. 4(b), it can be seen that an enhancement factor of 1.5–2.5 can be obtained around 282, 371, and 406 GHz.

These numerical results indicate that the photon DOS can be redistributed through electromagnetic band engineering, thus leading to enhanced thermal radiation in, for instance, a desired THz frequency range. However, at room temperature, the normal blackbody radiation power peaks at IR frequencies; and, as a result, the fraction of the total radiated thermal power in the THz region is very small. Even at 1000 K, the total radiance in the frequency range from 0.5 to 1.0 THz is less than 10 μW/cm^2/sr. Therefore, the enhancement factor of around 10 predicted above for the simple silicon and tungsten WPSs will not be sufficient for realizing a high power THz source. Nonetheless, a THz EBG object will certainly have a distinct thermal signature; and, consequently, it will be useful in thermal imaging and identification applications. In addition, advanced electromagnetic band engineering techniques may be used to dramatically increase the photon DOS of an object and, hence, dramatically increase the thermal radiation power enhancement factor to orders of magnitude higher in a narrow band of frequencies in the desired THz range. This dramatic enhancement factor can be achieved with resonant cavity arrays.

C. Metallodielectric Photonic Cavity

A special type of EM crystal that is based on a unit cell consisting of a metallic micro-cavity will produce the desired large enhancement factors. It is well-known that those metallic micro-cavities can result in very narrow lines in their emission spectra at certain optical frequencies, and that those resonant frequencies can be controlled by appropriate cavity size adjustments [42]–[44]. By properly designing the micro-cavities, similar resonant emissions can be achieved at THz frequencies.

We consider here cubic dielectric boxes surrounded by metallic walls to achieve enhanced THz emissions. The schematic diagram given in Fig. 5(a) shows the basic configuration. The unit cell of this quasi-3D structure is demarked by the dotted lines. The top metal layer will have either a thickness that is on the same order of its skin depth at the frequency of interest or a small aperture so that the resonant EM wave trapped in the micro-cavity can evanescently leak out [20].

According to theory, the only electromagnetic waves that can exist in a cavity have the specific wavelengths given by the expression

$$\lambda_{klm} = \frac{2na}{\sqrt{k^2 + l^2 + m^2}} \tag{5}$$

where n is the refractive index of the dielectric material filling the cavity, a is the side-length of the cavity, and the k, l and m indices are either zero or positive integers, but at least two of them should be nonzero [45]. These specific wavelengths are called the resonant wavelengths of the cavity. The largest one, for which two of the indices are unity and the other one is zero, is called the cutoff wavelength for the 110-mode and is given by $\lambda_{\text{cutoff}} = \sqrt{2}na$. Between the cutoff wavelength and an infinitely long wavelength, no electromagnetic wave is allowed to exist in the cavity. This behavior is analogous to an EBG structure. Due to the photon statistics, the amount of thermal radiation power at longer wavelengths is much larger than the values at shorter wavelengths. Thus, the mode at the cutoff wavelength is dominant over all of the other resonant modes and is the fundamental mode we focus on for the potential EM crystal-based THz source.

To demonstrate these effects, we considered an array of metallic box micro-cavities, each with the side-length $a = 141$ μm and filled with a dielectric material having a refractive index $n = 1.5$. We calculated the thermal radiation intensity at the cutoff frequency 1 THz (300 μ m wavelength). The radiation comes from two parts: one is the thermal emission from the dielectric box, whose DOS is denoted by $\rho_d(\lambda)$, and the other is from the surrounding metal walls. The latter wall

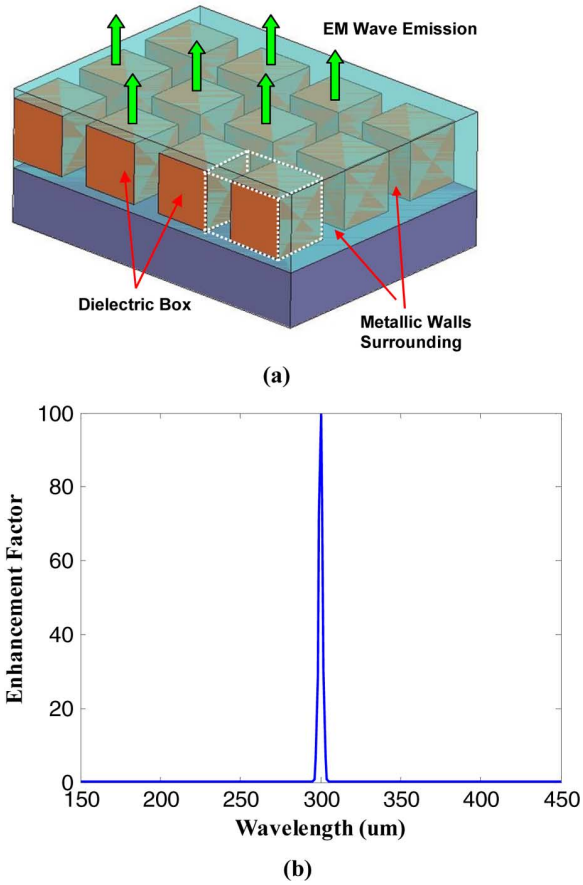

Fig. 5. (a) A schematic drawing of the metallic micro-cavities. The dotted lines enclose one unit cell of the structure. (b) The predicted thermal radiation power enhancement factor assuming a 1% variation in the size of the micro-cavities.

contributions follow Planck's Law. The total radiated thermal power density is then given by the expression

$$u(\lambda)d\lambda = \left(V_d\rho_d(\lambda) + V_m\frac{8\pi}{\lambda^4}\right)\frac{hc/\lambda}{e^{hc/\lambda kT}-1}d\lambda \tag{6}$$

where V_d and V_m are, respectively, the total volumes of the dielectric box and the metal wall. All other physical constants are the same as indicated in (1). Ideally, the DOS $\rho_d(\lambda)$ would be a delta function if the sizes of all the boxes were exactly identical. In practice, the box size variations due to fabrication tolerances widen the DOS $\rho_d(\lambda)$. For our calculations, we treated it as a Gaussian function with a full-width half-maximum (FWHM) of 1% of the cutoff wavelength 300 μm. Therefore, we obtained

$$\rho_d(\lambda) = \frac{N_{\text{res}}}{\sqrt{\pi/a}}e^{-t(\lambda-\lambda_0)^2}$$

where

$$t = \frac{0.693}{(\text{FWHM}/2)^2}. \tag{7}$$

In (7), N_{res} is the total number of states at the lowest resonant frequency; it is equal to 3 due to the 3-fold degeneracy of the indices k, l and m. The aspect ratio V_d/V_m is another critical quantity that determines the thermal radiation power density for the micro-cavity array. It is taken to be 12 here, a reasonable value for typical fabrication processes. The thermal radiation power enhancement factor of this whole structure is given by

$$\text{Enhancement factor} = \frac{V_d\rho_d(\lambda) + V_m\cdot 8\pi/\lambda^4}{(V_d+V_m)\cdot 8\pi/\lambda^4}. \tag{8}$$

The calculated result is plotted in Fig. 5(b). An enhancement of 100 times over the normal blackbody radiation value was obtained. As anticipated, the power output is quite narrowband. The FWHM of 1% of the cutoff wavelength is roughly equivalent to a variation in the box size of 3μm, an easily achievable one with standard fabrication processes such as photolithography and reactive ion etching [46]–[48].

In realistic scenarios, losses in the dielectric and the surrounding metal of the cavity will further broaden the thermal radiation spectrum. They can be taken into consideration by calculating the quality factor Q of the cavity at its cutoff frequency, given the cavity dimensions and material properties. The modified radiation FWHM including losses would be a combination of the FWHM from the cavity size variation and the FWHM from the losses (f_{cutoff}/Q). A cavity filled with polyethylene ($n = 1.52$ and loss tangent $= 0.001$ for the frequency band of interest here [49]) and with Platinum ($\sigma = 9.3e7$ Siemens/m) walls was simulated in HFSS. The dielectric cubic box was 141 μm on each side, and the metal wall thickness between adjacent boxes was set to be 11.3 μm. These choices gave an aspect ratio of about 12. The thickness of the top metal cover was chosen to be 180 nm, only slightly thicker than the Platinum skin depth at 1 THz. The simulation results show that this cavity has a quality factor $Q \sim 285$. This corresponds to a FWHM of 0.35%. Including the material losses of the micro-cavities, we found that the peak value of the enhancement factor was reduced and the width of the thermal emission peak shown in Fig. 5(b) was widened by about 35%.

IV. Fabrication and Characterization of the Silicon WPS

To verify our design and the fabrication process, a silicon WPS with the aforementioned dimensions was fabricated using a simple but robust mechanical layer-by-layer dicing process [50], [51]. A series of grooves were cut into both the front and back faces of a silicon wafer (with a resistivity of ~20 Ohm-cm) by using a diamond dicing saw. The depth of the cut was set to open a window at the crossing point of the cuts, but to leave the array joined at the crossing points of the resulting bars. One wafer thus makes up one half of the WPS unit cell shown in Fig. 1. The DISCO DAD320 dicing saw used here has horizontal and vertical step resolutions of 0.2 μm and 1.0 μm, respectively. In addition, its horizontal and vertical minimum positioning accuracies are 2.5 μm and 1.0 μm, respectively. Thus the estimated fabrication tolerances should be less than 5 μm in the x- and y-dimension and less than 2.0 μm in the z-dimension. The complete WPS is then assembled by stacking many wafers together with the help of pre-registered alignment marks. Fig. 6 is a photograph of the fabricated silicon WPS. Characterization of this EBG sample at THz frequencies was carried out

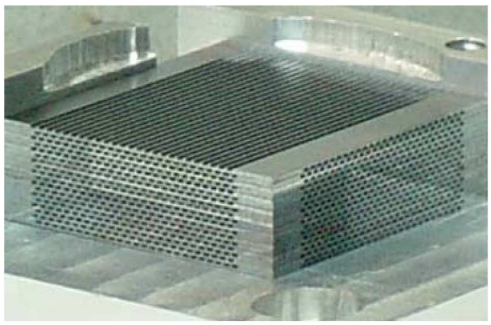

Fig. 6. A photograph of the fabricated silicon woodpile electromagnetic crystal.

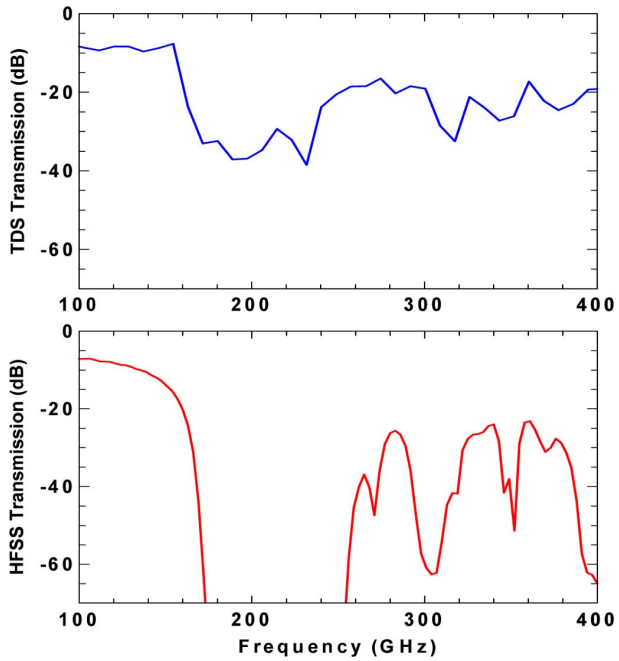

Fig. 7. Transmission responses (normal incidence) of the silicon WPS sample: (top) THz-TDS measurement, (bottom) HFSS Simulation.

with the THz time domain spectroscopy (THz-TDS) transmission approach. The measured and HFSS simulated transmission results along the sample stacking direction are shown in Fig. 7.

In the THz-TDS measurements, the silicon WPS was placed in the path of a pico-second pulse of THz radiation, and the pulse time history was compared with a reference signal (no sample being present). Then by Fourier transforming the signal transmitted through the sample, the sample transmission coefficient was obtained in frequency domain. The TDS result explicitly shows the predicted stop-band centered around 200 GHz. Also plotted in Fig. 7 is the HFSS simulated transmission coefficient for normal incidence. Not only does the predicted 200 GHz band gap match well, but also the predicted secondary band gap near 310 GHz and the various predicted transmission peaks match quite well with the measured data. The slight red shift observed in all of the features in the TDS spectrum with respect to the simulation is probably due to errors associated with the fabrication tolerances. Oblique incidence transmission measurements were performed; the results (not shown) verify that the band gap at 200 GHz is omnidirectional (a true 3-D band gap). The good agreement between the measured and simulated transmission results verifies the WPS design and fabrication procedures.

V. Thermal Radiation Measurements of the Silicon WPS

To experimentally study the predicted THz thermal radiation enhancement, direct thermal emission measurements of the fabricated silicon WPS were performed using a Beckman FS-720 Fourier Transform Spectrometer (FTS) with a frequency range from 100 to 3.6 THz. The FTS used a scanning Michelson interferometer to transform the incoming radiation into an amplitude-modulated signal whose modulation frequencies were the scaled-down frequencies in the original signal. The modulated signal was recorded as an interferogram and the original spectrum was then recovered by Fourier transformation. The maximum resolution of the FTS used in this work was 4.5 GHz. The schematic of the experimental configuration is shown in Fig. 8. The commonly used mercury lamp source for an FTS was replaced by the silicon WPS sample under study. For comparison, a THz radiation-absorption-material (RAM) [52] with an absorption coefficient close to 1 from 100 to 600 GHz and the same form factors as the WPS sample was used as the reference (control) blackbody source. A liquid helium cooled (4.2 K) silicon composite bolometer (IR Labs model JPKI06MA) was used as the signal detector, and a lock-in amplifier (SR510 m) was employed to enhance the measurement sensitivity.

The sample was mounted on an adjustable stage with a sample holder, an aperture, and an electrical heating element. The aperture, which was made from aluminum, blocks thermal emission from the sample except at the center aperture. The latter had a diameter of 0.64 cm, making the sample under study a good point source for the FTS collimator. A mechanical chopper was located in between the collimator and the aperture and was used as the reference of the lock-in amplifier. The thermal radiation from the sample was modulated by the chopper and passed through the FTS. It was detected by the cooled bolometer, which was positioned right behind the FTS output window. The optical beam path was located in a vacuum environment (except between the FTS output window and the bolometer) to reduce signal fluctuations caused by atmosphere. The heating element was directly attached to the aluminum sample holder, and the holder was kept in good thermal contact with the sample under study while being thermally isolated from the stage. A closed-loop thermal-couple temperature controller was used to maintain the sample to within 0.1 Kelvin of a specified constant temperature. Since the temperature sensor was mounted on the sample holder, the actual sample temperatures were carefully calibrated because of the different thermal conductivities of the holder and of the different samples (the silicon WPS and the RAM), which inevitably lead to a temperature gradient.

The detector sees the sample thermal radiation when the chopper is open and the chopper thermal radiation when it is closed. Because of the working principles of the lock-in amplifier, the detected signal is proportional to the power difference between the sample radiation and the chopper radiation. The final emission spectrum recorded by the FTS was therefore $W_{\mathrm{sample}}(f) - W_{\mathrm{chopper}}(f)$, where the suffix denotes

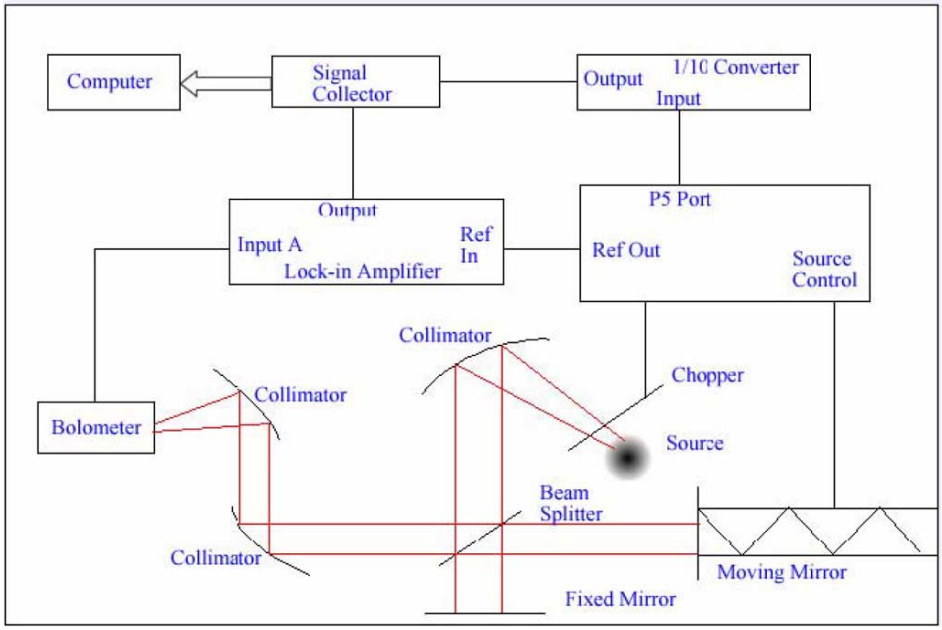

Fig. 8. Schematic of the FTS setup for the direct thermal emission measurements.

the specific radiation source. In addition, the recorded signal consists of the sample thermal emission, the thermal emission from the heating element transmitted through the sample, the background thermal emission reflected by the sample into the FTS, and the thermal emission from the aperture. The recorded differential spectrum can then be expressed as the following:

$$W(f,T_s) = \varepsilon_s \cdot W_{\mathrm{BB}}(f,T_s) + R_s \cdot W_{\mathrm{SUR}}(f,T_{\mathrm{RT}}) + X_s \cdot W_{\mathrm{HE}}(f,T_s) + W_{\mathrm{Aperture}}(f,T_{\mathrm{RT}}) - W_{\mathrm{Chopper}}(f,T_{\mathrm{RT}}) \quad (9)$$

where ε_s, R_s, and X_s are the emission, reflection, and transmission coefficients of the sample, respectively, and T_{S} and T_{RT} are the sample and room temperatures. The first term in (9) represents the thermal emission from the sample, where W_{BB} is the normal blackbody radiation power density at the sample temperature T_{s}. The second term represents the thermal radiation from the surrounding environment (W_{SUR}) that is reflected by the sample into the FTS. Since the heating stage is thermally isolated from the surrounding environment, the surrounding environment is at room temperature T_{RT}. The third term is the thermal radiation from the heating element (W_{HE}) transmitted through the sample at temperature T_{s}. The last two terms are the thermal radiations from the aperture (W_{Aperture}) and the chopper (W_{Chopper}). One thing to point out is that ε_s, R_s, and X_s are all considered to be independent of the temperature, which is a valid assumption over the studied temperature range.

In order to compare the thermal emissions from the silicon WPS and the RAM samples, the background signals from the surrounding environment, the heating element, the aperture, and the chopper were eliminated. This was achieved by subtracting the measured spectrum at room temperature T_{RT} from the measured spectrum at an interested higher temperature T_{s}. This way the second, fourth, and fifth terms in (9) are calibrated out, and the resulting spectrum is then

$$\Delta W = W(f,T_s) - W(f,T_{\mathrm{RT}}) = \varepsilon_s \cdot (W_{\mathrm{BB}}(f,T_s) - W_{\mathrm{BB}}(f,T_{\mathrm{RT}})) + X_s \cdot (W_{\mathrm{HE}}(f,T_s) - W_{\mathrm{HE}}(f,T_{\mathrm{RT}})). \quad (10)$$

This expression is a combination of the sample thermal emission and the heating element thermal emission transmitted through the sample. According to the THz-TDS transmission measurement, the transmission coefficient of the RAM can be well approximated to be zero. Therefore the RAM differential spectra represent the RAM thermal emissions. In addition, from Fig. 7, it is observed that the power transmission through the silicon WPS was also quite low (less than -10 dB for most of the spectrum). Therefore, the second term in (10) can also be omitted. A comparison of the WPS and RAM emissions is given in Fig. 9 by plotting the ΔW (in arbitrary units) obtained for both the silicon WPS and the RAM samples. This comparison is fair since the term $W_{\mathrm{BB}}(f,T_s) - W_{\mathrm{BB}}(f,T_{\mathrm{RT}})$ in (10) is a constant factor for both the WPS and the RAM samples at the same temperature.

The thermal radiation results measured at two different temperatures (38°C and 85°C) are plotted in Fig. 9. Because the absolute thermal emission power at these temperatures were low and the sensitivity of the FTS system was not optimal at the lower frequency end (100 to 500 GHz) [53], all of the emission spectra were measured multiple times and averaged to reduce the noise level. The error bars in Fig. 9 represent the statistical measurement errors.

Experimentally measured enhancements of the WPS thermal radiation over the control blackbody sample can be observed around 110, 146, 165, 288, 362 and 440 GHz for the 85°C spectrum. Enhancements at similar frequencies are also seen for the

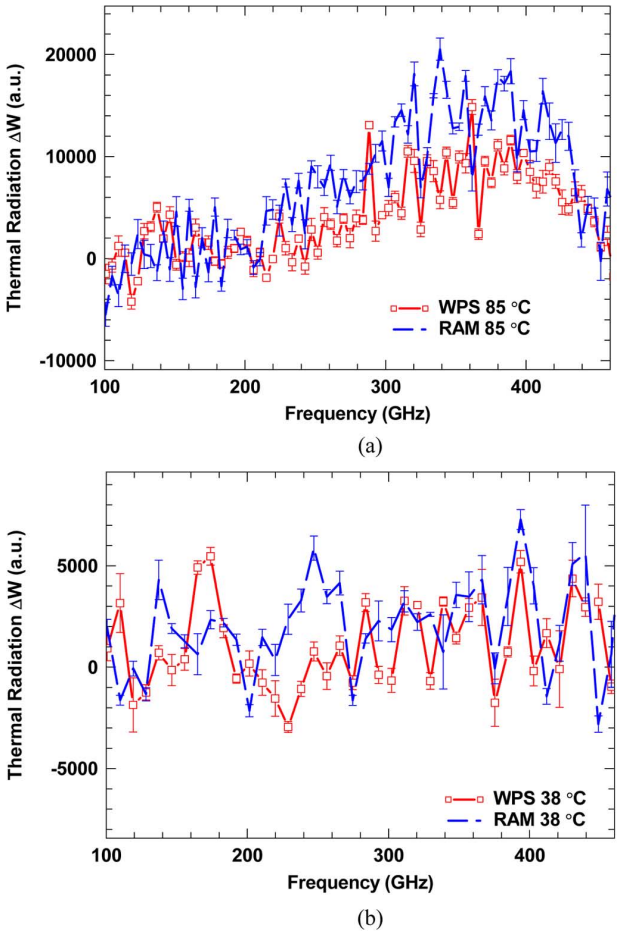

Fig. 9. The thermal radiation differential spectra for the RAM (dashed) and the WPS (squares) samples at (a) 85°C and (b) 38°C. The error bars are statistical.

38°C spectrum. These enhancement peaks match up qualitatively well with the predicted enhancement peak positions given in Fig. 2(c). Consider the most significant enhancement peak at 364 GHz in Fig. 2(c) as an example, a sharp enhancement peak at 362 GHz is observed in the measured 85°C spectrum [see Fig. 9(a)]. An enhancement peak in the 38°C spectrum [Fig. 9(b)] appears at 340 GHz, instead of at 360 GHz. This discrepancy is probably due to the relatively low frequency resolution of the data (9 GHz instead of the 4.5 GHz for the 85°C spectrum) and the relatively low signal-to-noise ratio (SNR) at the lower temperature of 38°C compared to the 85°C. Besides the main enhancement peak, other frequencies at which enhancement peaks occur also qualitatively match well with the predictions in Fig. 2. The measured thermal radiation spectra in Fig. 9 look quite noisy because of the limited SNR in the measurements at this frequency range. However, statistical error bars verify that the measured WPS emission enhancements over the control blackbody sample are repeatable observations. Therefore, based on the good matching between the predicted and measured (for both temperatures) enhancement peak frequencies, the results shown in Fig. 9 justify, at least qualitatively, the prediction of the thermal radiated power using the DOS calculation. They are also good indications that an EBG emission source with enhanced THz thermal radiation may be feasible. Quantitative comparison between the measured and the predicted values was not attempted, since the measurement sensitivity is not high enough at this frequency range.

In order to verify, as predicted, that the observed enhancement was a total thermal radiation power enhancement over the entire 4π solid angle sphere, emission measurements covering the entire space were required. In the experiment reported here, the power detection was confined within a 0.11π solid angle along the sample surface normal direction. However, transmission and reflection characterizations of a scaled-down WPS at optical frequencies have been reported previously with minimal angular variances [36], [54]. The oblique incidence THz-TDS transmission characterization of the WPS sample used in this work also showed small angular variance. Therefore, it is reasonable to assume that the thermal radiation enhancement should not have a strong angular dependence. It is worth emphasizing that the thermal radiation enhancement predicted in Fig. 2 is a total power enhancement in the THz regime based on the calculation of the DOS for the WPS sample, and that the measured WPS emission enhancements along the surface normal direction support those calculations.

VI. Conclusion and Discussion

In this paper we presented a novel idea of modifying THz thermal emission spectra by using different types of EBG crystals as the active THz sources. It was demonstrated that large enhancements over normal blackbody radiation may be achieved with the large redistribution of the photon DOS enabled by the EBG effects associated with an EM crystal. These enhancement factors were shown to be independent of the temperature. The design and fabrication of a silicon woodpile crystal were also accomplished. The silicon WPS sample was characterized by the THz-TDS transmission spectroscopy method; and the results agreed well with the simulation values.

Direct thermal emission measurements were carried out with the fabricated silicon woodpile sample and a RAM sample (approximately a blackbody radiator) as the sources. Emission enhancements of the WPS over the RAM were observed at certain frequencies. These enhancements occurred at frequencies similar to those predicted by the photon DOS calculations. The observed enhancements are a good indication that properly engineered EM crystals may lead to an alternative THz thermal source.

In the future, structures other than the silicon WPS, such as the tungsten WPS and the metallic micro-cavity array, will be designed with optimized thermal emissions in the THz region to achieve higher total thermal radiated powers. Also, dual-gap or even multiple gap EM crystals will be investigated, and their thermal radiation characteristics will be explored. Multiple gaps would result in much stronger photon DOS redistributions and possibly much higher thermal radiated power enhancements over the normal blackbody values than could be realized with single gap EBG structures. In addition, the possibility of making the proposed sources tunable will be explored. Since the stop-band positions within an EM crystal is largely dependent on the refractive index n of its constitutive material, and since the refractive indices of certain materials such as semiconductors or liquid crystals can be controlled by external biases, we believe that tunable EM crystal-based THz sources

are possible. If the feasibility of making EM crystals with such materials is confirmed, tunable THz radiation achieved by a tunable n would be quite interesting. Future theoretical and experimental work may lead to a promising alternative type of THz source, as well as to a better understanding of the physics underlying thermal power radiated by an EM crystal.

ACKNOWLEDGMENT

The authors would like to thank Dr. C. Walker at the University of Arizona for help in the FTS emission measurement and Dr. D. Barker for help in the sample preparation, and the Submillimeter-wave Technology Laboratory, University of Massachusetts, Lowell, for providing the radiation absorption material (RAM) as the blackbody control.

REFERENCES

[1] P. H. Siegel, "Terahertz technology," *IEEE Trans. Microw. Theory Tech.*, vol. 50, pp. 910–928, Mar. 2002.

[2] J. W. Fleming, "High resolution submillimeter-wave Fourier-transform spectrometry of gases," *IEEE Trans. Microw. Theory Tech.*, vol. 22, pp. 1023–1025, Dec. 1974.

[3] R. J. Dengler, A. Skalare, and P. H. Siegel, "Passive and active imaging of humans for contraband detection at 640 GHz," in *IEEE MTT-S Int. Microwave Symp. Digest*, Jun. 2004, vol. 3, pp. 1951–1594.

[4] J. R. Ashley and F. M. Palka, "Transmission cavity and injection stabilization of an X-band transferred electron oscillator," in *IEEE MTT-S Int. Microwave Symp. Digest*, Jun. 1973, vol. 73, pp. 181–182.

[5] E. J. Nichols and J. D. Tear, "Joining the infrared and electric wave spectra," *Astrophys. J.*, vol. 61, pp. 17–37, Jan. 1925.

[6] P. Coleman, "State of the art: Background and recent developments—millimeter and submillimeter waves," *IEEE Trans. Microw. Theory Tech.*, vol. 11, pp. 271–288, Sep. 1963.

[7] P. H. Siegel, "Terahertz technology in biology and medicine," *IEEE Trans. Microw. Theory Tech.*, vol. 52, pp. 2438–2447, Oct. 2004.

[8] A. Straprans, E. McCune, and J. Ruetz, "High-power linear-beam tubes," *Proc. IEEE*, vol. 61, pp. 299–330, Mar. 1973.

[9] E. R. Mueller, "Submillimeter wave lasers in," in *Wiley Encyclopedia of Electrical and Electronics Engineering*. New York: Wiley, 1999, vol. 20, pp. 587–615.

[10] A. V. Raisanen, "Frequency multipliers for millimeter and submillimeter wavelengths," *Proc. IEEE*, vol. 80, pp. 1842–1852, Nov. 1992.

[11] X. Melique, C. Mann, P. Mounaix, J. Thornton, O. Vanbesien, F. Mollot, and D. Lippens, "5-mW and 5% efficiency 216-GHz InP-based heterostructure barrier varactor tripler," *IEEE Microw. Guided Wave Lett.*, vol. 8, pp. 384–386, Nov. 1998.

[12] A. Maestrini, J. S. Ward, J. J. Gill, H. S. Javadi, E. Schlecht, C. T-Canseliet, G. Chattopadhyay, and I. Mehdi, "A 540–640-GHz high-efficiency four-anode frequency tripler," *IEEE Trans. Microw. Theory Tech.*, vol. 53, pp. 2835–2843, Sep. 2005.

[13] E. R. Brown, F. W. Smith, and K. A. McIntosh, "Coherent millimeter-wave generation by heterodyne conversion in low-temperature-grown GaAs photoconductors," *J. Appl. Phys.*, vol. 73, pp. 1480–1484, Feb. 1993.

[14] Z.-Y. Li, "Modified thermal radiation in three-dimensional photonic crystals," *Phys. Rev. B*, vol. 66, pp. 241103–241106, Dec. 2002.

[15] C.-H. Chao, C.-Y. Kang, and C.-F. Lin, "Theoretical calculation for the visible light enhancement of the black-body radiation of metallic photonic boxes," in *Optics and Photonics*, Tainan, Taiwan, Dec. 2005.

[16] W. W. Chow, "Theory of emission from an active photonic lattice," *Phys. Rev. A*, vol. 73, pp. 013821–013829, Jan. 2006.

[17] I. El-Kady, W. W. Chow, and J. G. Fleming, "Emission from an active photonic crystal," *Phys. Rev. B*, vol. 72, pp. 195110–195114, Nov. 2005.

[18] I. Celanovic, F. O'Sullivan, M. Ilak, J. Kassakian, and D. Perreault, "Design and optimization of one-dimensional photonic crystals for thermophotovoltaic applications," *Opt. Lett.*, vol. 29, pp. 863–865, Apr. 2004.

[19] S.-Y. Lin, J. G. Fleming, E. Chow, J. Bur, K. K. Choi, and A. Goldberg, "Enhancement and suppression of thermal emission by a three-dimensional photonic crystal," *Phys. Rev. B*, vol. 62, pp. R2243–R2246, Jul. 2000.

[20] C.-F. Lin, C.-H. Chao, L. A. Wang, and W.-C. Cheng, "Blackbody radiation modified to enhance blue spectrum," *J. Opt. Soc. Am. B*, vol. 22, pp. 1517–1520, Jul. 2005.

[21] C. M. Cornelius and J. P. Dowling, "Modification of Planck blackbody radiation by photonic band-gap structures," *Phys. Rev. A*, vol. 59, pp. 4736–4746, Jun. 1999.

[22] A. Narayanaswamy and G. Chen, "Thermal emission control with one-dimensional metallodielectric photonic crystals," *Phys. Rev. B*, vol. 70, pp. 125101–125104, Sep. 2004.

[23] C. Luo, A. Narayanaswamy, G. Chen, and J. D. Joannopoulos, "Thermal radiation from photonic crystals: A direct calculation," *Phys. Rev. Lett.*, vol. 93, pp. 213905–213908, Nov. 2004.

[24] T. Trupke, P. Wurfel, and M. A. Green, "Comment on 'Three-dimensional photonic-crystal emitter for thermal photovoltaic power generation'," *Appl. Phys. Lett.*, vol. 84, pp. 1997–1998, Mar. 2004.

[25] S. Noda, K. Tomoda, N. Yamamoto, and A. Chutinan, "Full three-dimensional photonic bandgap crystals at near-infrared wavelengths," *Science*, vol. 289, pp. 604–606, Jul. 2000.

[26] H. Han, H. Park, M. Cho, and J. Kim, "Terahertz pulse propagation in a plastic photonic crystal fiber," *Appl. Phys. Lett.*, vol. 80, pp. 2634–2636, Apr. 2002.

[27] D. Arnone, "10 emerging technologies that will change your world," *Technol. Rev.*, vol. 107, pp. 32–51, Feb. 2004.

[28] E. Yablonovich, "Inhibited spontaneous emission in solid-state physics and electronics," *Phys. Rev. Lett.*, vol. 58, pp. 2059–2062, May 1987.

[29] M. Planck, *The Theory of Heat Radiation*. New York: Dover, 1959.

[30] S.-Y. Lin, J. Moreno, and J. G. Fleming, "Three-dimensional photonic-crystal emitter for thermal photovoltaic power generation," *Appl. Phys. Lett.*, vol. 83, pp. 380–382, Jul. 2003.

[31] S.-Y. Lin, J. Moreno, and J. G. Fleming, "Response to comment on three-dimensional photonic-crystal emitter for thermal photovoltaic power generation," *Appl. Phys. Lett.*, vol. 84, p. 1999, Mar. 2004.

[32] S.-Y. Lin, J. G. Fleming, and I. El-Kady, "Three-dimensional photonic-crystal emission through thermal excitation," *Opt. Lett.*, vol. 28, pp. 1909–1911, Oct. 2003.

[33] J. G. Fleming, "Addendum: "Three-dimensional photonic-crystal emitter for thermal photovoltaic power generation," *Appl. Phys. Lett.*, vol. 86, pp. 249902–249903, Jun. 2005.

[34] C. H. Seager, M. B. Sinclair, and J. G. Fleming, "Accurate measurements of thermal radiation from a tungsten photonic lattice," *Appl. Phys. Lett.*, vol. 86, pp. 244105–244107, Jun. 2005.

[35] J.-H. Lee, Y.-S. Kim, K. Constant, and K.-M. Ho, "Woodpile metallic photonic crystals fabricated by using soft lithography for tailored thermal emission," *Adv. Mater.*, vol. 19, pp. 791–794, Feb. 2007.

[36] S.-Y. Lin, J. G. Fleming, D. L. Hetherington, B. K. Smith, R. Biswas, K.-M. Ho, M. M. Sigalas, W. Zubrzycki, S. R. Kurtz, and J. Bur, "A three-dimensional photonic crystal operating at infrared wavelengths," *Nature*, vol. 394, pp. 251–253, Jul. 1998.

[37] S. G. Johnson and J. D. Joannopoulos, "Block-iterative frequency-domain methods for Maxwell's equations in a planewave basis," *Opt. Express*, vol. 8, pp. 173–190, Jan. 2001.

[38] G. Lehmann and M. Taut, "On the numerical calculation of the density of states and related properties," *Phys. Stat. Sol. (b)*, vol. 54, pp. 469–477, Jul. 1972.

[39] O. Jepson and O. K. Anderson, "The electronic structure of H. C. P Ytterbium," *Solid State Commun.*, vol. 9, pp. 1763–1767, Jan. 1971.

[40] High Frequency Structure Simulator, Version 10 2005, Ansoft Corporation.

[41] R. C. Jaeger, "Thermal oxidation of silicon," in *Introduction to Microelectronic Fabrication*. Upper Saddle River, NJ: Prentice Hall, 2002.

[42] F. Kusunoki, J. Takahara, and T. Kobayashi, "Qualitative change of resonant peaks in thermal emission from periodic array of microcavities," *Electron. Lett.*, vol. 39, pp. 23–24, Jan. 2003.

[43] F. Kusunoki, T. Kohama, T. Hiroshima, S. Fukumoto, J. Takahara, and T. Kobayashi, "Narrow-band thermal radiation with low directivity by resonant modes inside tungsten microcavities," *Jpn. J. Appl. Phys.*, vol. 43, no. 8A, pp. 5253–5258, Aug. 2004.

[44] H. Yokoyama, "Physics and device application of optical microcavities," *Science*, vol. 256, pp. 66–70, Apr. 1992.

[45] D. K. Cheng, *Field and Wave Electromagnetics*, 2nd ed. New York: Addison-Wesley, 1989.

[46] S. Maruyama, T. Kashiwa, H. Yugami, and M. Esashi, "Thermal radiation from two dimensionally confined modes in microcavities," *Appl. Phys. Lett.*, vol. 79, pp. 1393–1395, Aug. 2001.

[47] M. Sugawara and B. L. Stansfield, *Plasma Etching: Fundamentals and Applications*. New York: Oxford Univ. Press, 1998.

[48] J. R. Sheats and B. W. Smith, *Microlithography: Science and Technology*. New York: Marcel Dekker, 1998.
[49] J. W. Lamb, "Miscellaneous data on materials for millimetre and submillimetre optics," *Int. J. Infrared Millimeter Waves*, vol. 17, pp. 1997–2034, Dec. 1996.
[50] R. Gonzalo, B. Martinez, C. M. Mann, H. Pellemans, P. H. Bolivar, and P. de Maagt, "A low-cost fabrication technique for symmetrical and asymmetrical layer-by-layer photonic crystals at submillimeter-wave frequencies," *IEEE Trans. Microw. Theory Tech.*, vol. 50, pp. 2384–2392, Oct. 2002.
[51] B. Martinez, I. Ederra, R. Gonzalo, B. Alderman, L. Azcona, P. G. Huggard, B. D. Hon, A. Hussain, S. R. Andrews, L. Marchand, and P. de Maagt, "Manufacturing tolerance analysis, fabrication, and characterization of 3-D submillimeter-wave electromagnetic-band gap crystals," *IEEE Trans. Microw. Theory Tech.*, vol. 55, pp. 672–681, Apr. 2007.
[52] R. H. Giles and T. M. Horgan, "Silicone-Based Wedged-Surface Radiation Absorbing Material," U.S. Patent Number 5 260 513, Nov. 9, 1993.
[53] H. Xin, Z. Wu, A. Young, and R. W. Ziolkowski, "THz thermal radiation enhancement using electromagnetic crystals," in *Proc. IEEE AP-S Int. Symp.*, Honolulu, HI, Jun. 9–15, 2007, pp. 2249–2252.
[54] J. G. Fleming, S.-Y. Lin, I. El-Kady, R. Biswas, and K.-M. Ho, "All-metallic three-dimensional photonic crystals with a large infrared bandgap," *Nature*, vol. 417, pp. 52–55, May 2002.

Hao Xin (SM'06) received the Ph.D. degree in physics from the Massachusetts Institute of Technology (MIT), Cambridge, in 2001.

He performed research studies for five years at MIT's Physics Department and at Lincoln Laboratory, where he investigated power dependence of the surface impedance of high-Tc superconducting films and Josephson junction properties at microwave frequencies. From November 2000 to November 2003, he was a Research Scientist with Rockwell Scientific Company, where he conducted research as Principal Manager/Principal Investigator in the area of electromagnetic band-gap surfaces, quasi-optical amplifiers, electronically scanned antenna arrays, MMIC designs using various III-V semiconductor compound devices, and random power harvesting. From 2003 to 2005, he was a Sr. Principle Multidisciplinary Engineer at Raytheon Missile Systems, Tucson, AZ. He is now an Assistant Professor of the Electrical and Computer Engineering Department and the Physics Department, University of Arizona, Tucson. He has published over 60 refereed technical papers in the areas of solid-state physics, photonic crystals, and the applications thereof in microwave and millimeter wave technologies. He has twelve patents issued and one pending in the areas of photonic crystal technologies, random power harvesting based on magnetic nano-particles, and microwave nano-devices. His current research focus is in the area of microwave, millimeter wave, and THz technologies, including solid state devices and circuits, antennas, passive circuits, and applications of new materials such as metamaterials and carbon nanotubes.

Ziran Wu was born in Hefei, China, in 1982. He received the B.Sc. degree in physics from the University of Science and Technology of China, Hefei, in 2004 and the M.Sc. degree in physics from the University of Arizona, Tucson, in 2006, where he is currently working toward the Ph.D. degree.

Since October 2005, he has been working in the Millimeter Wave Circuits and Antennas Laboratory, Electrical and Computer Engineering Department, University of Arizona. His main research work includes THz thermal radiation enhancement with electromagnetic bandgap material, carbon nanotube THz characterization and THz carbon nanotude device development, THz EBG material, components and devices rapid prototyping, and development of Microwave testing device and active device.

Abram Young received the B.Sc. degree in physics from the University of Arizona, Tucson, in 1998.

He then worked as a Physicist at Raytheon, Tucson, AZ, in such diverse areas as laser remote sensing, positron annihilation spectroscopy, and novel applications of photonic bandgap devices from millimeter wave to optical regimes where he was the author and coauthor of several patents. He is currently a Visiting Scholar in the Accelerator Mass Spectrometry Group in physics at the University of Arizona. In addition, he is also working at TeraVision, Inc.,Tuscon, AZ, on sub-millimeter wave device physics.

Richard W. Ziolkowski (M'97–SM'91–F'94) received the Sc.B. degree in physics (*magna cum laude* with honors) from Brown University, Providence, RI, in 1974 and the M.S. and Ph.D. degrees in physics from the University of Illinois at Urbana-Champaign, in 1975 and 1980, respectively.

He was a member of the Engineering Research Division, Lawrence Livermore National Laboratory, from 1981 to 1990 and served as the Leader of the Computational Electronics and Electromagnetics Thrust Area for the Engineering Directorate from 1984 to 1990. He joined the Department of Electrical and Computer Engineering, University of Arizona, Tuscon, as an Associate Professor in 1990, and was promoted to Full Professor in 1996. He was selected by the Faculty to serve as the Kenneth Von Behren Chaired Professor for 2003 to 2005. He currently is serving as the Litton Industries John M. Leonis Distinguished Professor. He holds a joint appointment with the College of Optical Sciences at the University of Arizona. His research interests include the application of new mathematical and numerical methods to linear and nonlinear problems dealing with the interaction of acoustic and electromagnetic waves with complex media, metamaterials, and realistic structures.

Prof. Ziolkowski is a Fellow of the Optical Society of America and a member of Tau Beta Pi, the American Physical Society, and Commissions B and D of URSI. He was awarded the Tau Beta Pi Professor of the Year Award in 1993 and the IEEE and Eta Kappa Nu Outstanding Teaching Award in 1993 and 1998. He served as the Vice Chairman of the 1989 IEEE/AP-S and URSI Symposium in San Jose, and as the Technical Program Chairperson for the 1998 IEEE Conference on Electromagnetic Field Computation. He was an Associate Editor for the IEEE TRANSACTIONS ON ANTENNAS AND PROPAGATION from 1992 to 1998. He served as a member of the IEEE Antennas and Propagation Society (AP-S) Administrative Committee (ADCOM) from 2000 to 2002, and is currently serving as a Past-President member. He served as the IEEE AP-S Vice President in 2004 and President in 2005. He was a Steering Committee Member for the 2004 ESA Antenna Technology Workshop on Innovative Periodic Antennas. He served as a Co-Chair of the International Advisory Committee for the inaugural IEEE International Workshop on Antenna Technology, IWAT2005, and since as a member of the International Advisory Committee for the IWAT Meetings. He was member of the International Advisory Committee for MAPE2005. He served as an Overseas Corresponding Member of the ISAP2007 Organizing Committee. He was a Co-Guest Editor for the October 2003 IEEE TRANSACTIONS ON ANTENNAS AND PROPAGATION Special Issue on Metamaterials. For the US URSI Society he served as Secretary for Commission B (Fields and Waves) from 1993 to 1996 and as Chairperson of the Technical Activities Committee from 1997 to 1999, and as Secretary for Commission D (Electronics and Photonics) from 2001 to 2002. He served as a Member-at-Large of the U.S. National Committee (USNC) of URSI from 2000 to 2002 and is now serving as a member of the International Commission B Technical Activities Board. He was a Co-Guest Editor of the 1998 special issue of *J. Opt. Soc. Am* featuring mathematics and modeling in modern optics. He was a Co-Organizer of the Photonics Nanostructures Special Symposia at the 1998, 1999, 2000 OSA Integrated Photonics Research (IPR) Topical Meetings. He served as the Chair of the IPR sub-committee IV, Nanostructure Photonics, in 2001.